Asian Journal of Chemistry; Vol. 24, No. 6 (2012), 2629-2633

ASIAN JOURNAL OF CHEMISTRY

www.asianjournalofchemistry.co.in

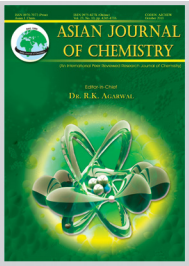

Novel Saucer-Shaped γ-Manganese Dioxides Nanoplates

DESHAN ZHENG

School of Materials and Chemical Engineering, Xi'an Technological University, Xi'an 710032, P.R. China

Corresponding author: Fax: +86 29 83208197; Tel: +86 29 83208197; E-mail: deshan.zheng@sdu.edu.cn

(*Received*: 7 June 2011; *Accepted*: 17 January 2012) AJC-10960

γ-Manganese dioxides with novel saucer-shaped hexagonal nanoplates structure have been successfully synthesized *via* a simple chemical route without the addition of any surfactants or organic templates. The hexagonal nanoplates have edge lengths about of 250 nm with the thickness only several tens of nanometers. By tracking the crystallization and morphology of the products at different reaction stages, we proposed a possible formation mechanism of this novel morphology of nanoplates. The present study offered a new, simple route for bulk synthesis of two-dimensional γ-MnO_2 nanoplates and enlarged the family of MnO_2 available.

Key Words: Nanostructures, Growth models, Crystal morphology, Hydrothermal crystal growth, Nanomaterials.

INTRODUCTION

The synthesis of novel nanostructures materials with controlled size and shape has always being stimulated great research interest in seeking novel properties and tailorable functions, since the physical properties of these materials may be depended not only on the compositions but also on the morphologies of the particles[1,2]. Nanostructures manganese dioxides as a well-known transition-metal oxide with different crystallographic forms and morphologies have attracted much attention due to their many important technological applications[3-10]. Among all the MnO_2 structures, perhaps the best-known polymorph is γ-MnO_2 that was considered as one of the most attractive cathode active materials for battery industry. Its electrical potential is reduced more slowly as comparing with the other forms during the discharge process and it also presents significant advantages in terms of the cost and environmental impact by contrasting with the cobalt oxide used in presently commercialized batteries. Due to the advantages of γ-MnO_2 as the cathode of battery, many researches have been prompted to prepare γ-MnO_2 with different microstuctures and the remarkable progress has been achieved. For example, Wang and Li[11] reported that γ-MnO_2 nanowires/nanorods were synthesized by a hydrothermal method based on the redox reactions of MnO_4^- and/or Mn^{2+}. In the works of Yuan *et al.*[12] single-crystalline nanowires of γ-MnO_2 were prepared by hydrothermally treating commercial γ-MnO_2 powders in water or ammonia solution. Xie and her co-workers synthesized γ-MnO_2 nanowires *via* a coordination-polymer-precursor route[13]. Suib's[14] and Xie's[15] groups also fabricated γ-MnO_2 hollow nanospheres and γ-MnO_2 microspheres, respectively.

However, there are only few reports on the synthesis of γ-MnO_2 single crystals so far. The reason is that the single crystal particles of γ-MnO_2 are difficult to synthesize comparing with other MnO_2 forms due to the fact that γ-phase is metastable and easily transformed to be the β-form during process of synthesis[11,16] and manganese oxide also has the strong tendency to precipitate or coagulate during the preparation process[17]. The literature reported that most of preparation procedures involved the reduction of salt permanganate or thermal decomposition of organometallic precursors in the presence of surfactants, polymers, biomolecules and coordinating ligands sometimes. Nevertheless, the permanganate route has a practical drawback: the high cost of permanganate. The major shortcomings of other organometallic precursors methods need to completely remove the templates, otherwise impurities will exist on the surfaces of the final products, which usually influences or restricts the applications of these metallic nanostructures. However, the removal of the residues from the particle surface requires harsh conditions or multiple washing. Therefore, for the properties studies and future applications of nanoscale materials, it is necessary to develop the simple, convenient and template-free synthetic method to obtain the new nanostructures with controllable morphologies and structures.

In this paper, we demonstrate a simple aqueous chemical route for the mass synthesis of the saucer-shaped hexagonal γ-MnO_2 nanoplates by the hydrothermal treatment of $Mn(NO_3)_2$ at 180 ºC. The preparation process was carried out without using any organic templates or surfactants, which avoided the subsequent complicated procedure for the removal of the

template or surfactants. To the best of our knowledge, there are few reports of this novel saucer-shaped hexagonal 2D γ-MnO_2 nanoplate prepared by a single-step hydrothermal reaction in published papers[18-20]. Furthermore, we also proposed a possible mechanism to explain the formation of this novel morphology of nanoplates.

EXPERIMENTAL

Sample preparation: In a typical synthesis procedure, $Mn(NO_3)_2{\cdot}4H_2O$ were dissolved in distilled water with vigorous stirring. When the solution was clarified, 12 mL aqueous solution containing 12 mmol $NaClO_3$ was added under continuous stirring. The resulting transparent solution was put into a Teflon-lined stainless steel autoclave and it was kept at 180 ºC for 20 h. After the reaction was completed, the solution was filter and the solid black precipitate was washed several times with distilled water and absolute ethanol, respectively. The obtained black powders were dried at 50 ºC in air.

Characterization: The samples were characterized by X-ray diffraction (XRD) using a Japan Rigaku D/Max-γA rotation anode X-ray diffractometer equipped with graphite-monochromatized Cu-K_α radiation (l = 1.54178 Å) at a scanning rate of 0.02º s^{-1} in the 2θ range from 10º to 75º. The morphologies and nanostructure of the as-synthesized saucer-shaped γ-MnO_2 hexagonal nanoplates were characterized by field emission scanning electron microscopy (FESEM JSM-6700F). Transmission electron microscopy was carried out using JEM-100CXII at an accelerating voltage of 100 kV. The samples for these measurements were dispersed in absolute ethanol by vibration in the ultrasonic pool. Then, the solutions were dropped onto a copper grid coated with amorphous carbon films and dried in air before performance.

RESULTS AND DISCUSSION

Crystal structure and morphology of γ-MnO_2 hexagonal nanoplates: Fig. 1 shows the X-ray diffraction of the samples formed at a hydrothermal treatment temperature of 180 ºC. The poor quality of X-ray diffraction patterns resulted from by low intensity and broad peaks indicated a high degree of disorder. As we all know, the important feature of the structure of γ-MnO_2 is a inhomogeneous host compound because it contains at least two chemically different Mn atoms located into the building blocks of ramsdellite and pyrolusite layers, respectively and the latter intergrowth within the former matrix, which the complex microstructure mainly includes De Wolff disorder, microtwinning and point defects. These structural defects are responsible for the complex and variable X-ray powder diffraction patterns of γ-MnO_2, such as the rather poor quality of the X-ray diffraction pattern (low intensity, broad lines and always consist mostly of small number of sharp and broad lines on top of a diffuse background) and also for their difficult characterization experimentally at the atomistic level. However, the materials with poor X-ray diffraction patterns can be further investigated using the local structural tools such as electron diffraction, by which the hexagonal nanoplates were shown as the single crystals, not amorphous or other impurities (Fig. 2d). By combinating the electron diffraction, it can be deduced reasonably that all of the reflection peaks of X-ray diffraction patterns are consistent with the pure orthorhombic phase of γ-MnO_2 (Joint Committee on Powder Diffraction Standards (JCPDS) card No.14-0644, a = 6.36 Å, b = 10.15 Å, c = 4.09 Å). There are no peaks observed corresponding to the impurities such as $Mn(OH)_2$ and $Mn(OH)_4$.

The morphology of the as-synthesized saucer-shaped hexagonal γ-MnO_2 nanoplates was characterized by transmission electron microscopy and field emission scanning electron microscopy. Fig. 1b shows that most of the nanoplates distribute on the substrate and exhibit the plate-like shape. Many nanoplates have regular edges with an angle of 120º between adjacent sides. It is well known that if all the inner angles of a planar polygon are 120º, their sides will be geometrically defined as a hexagon, no matter the lengths of their sides are equal (perfect hexagons) or not (deformed hexagons). Therefore, we can clearly observe that the included angle between two neighbouring sides of all the plates are 120º. Although a few nanoplates show the deformed hexagons, many nanoplates preserved the shape of well-defined hexagonal morphology just as shown in the magnification image (Fig. 1c). The most impressive feature of the surface of nanoplates is not flat, instead, ridges and concave can be identified and resulting in the formation of concaves on the surface of the hexagonal γ-MnO_2 nanoplates, which uneven-surface feature of nanoplates can be deduced from their high and inconsistent contrast of the transmission electron images.

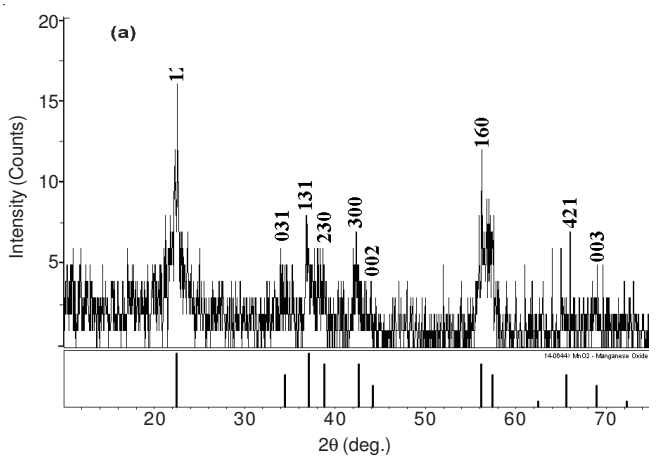

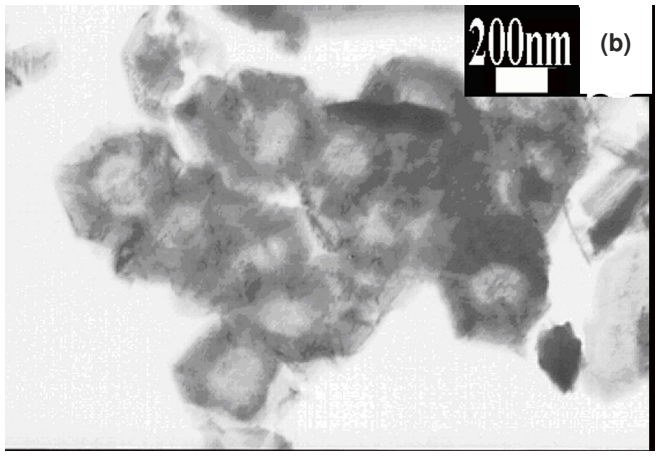

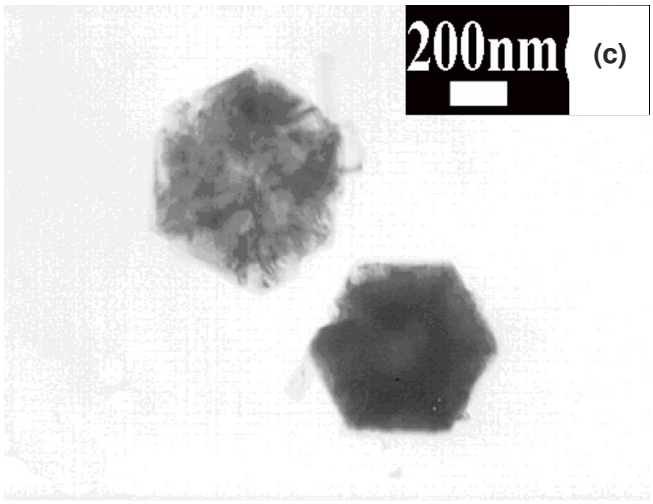

Fig. 1. X-ray diffraction pattern of the as-prepared γ-MnO_2 nanoplatelets (a) and the transmission electron images of samples (b) and (c)

This feature of formation of concaves on the surface of the hexagonal γ-MnO_2 nanoplates can be further illustrated by the low- and high-magnification scanning electron images, as shown in Fig. 2(a-b). From Fig. 2a, it was observed that there are large amount of hexagonal plate-like γ-MnO_2 nanoplates. The scanning electron image with higher magnification (Fig. 2b) reveals that most of the γ-MnO_2 products entirely consist of nanometer-scale plates with the thickness of several tens of nanometers. The side length is between 200 nm and 1 μm. The aspect ratio of diameter-to-thickness is about 8 ± 2. In spite of the difference in their edge length, most of the nanoplates possess the well-defined hexagonal structure with sharp edges. Interestingly, there is a concave on the top surface of each microparticle, which forms the novel saucer-shaped hexagonal nanoplates. In addition, a proportion of the nanoplates exhibit multilayered morphology except for some monolayer nanoplates (arrow a) and the profile of morphology looks like a Hamburger (arrow b) that is usually composed of several layers in the range from 3 to 8. The thicknesses of nanoplates are approximately 28±10 nm. Inset of Fig. 2b gives a magnified typical image of such multilayered three-dimensional structure. From the top view of the multilayered structure, the layers of assembled nanosheets in the 3D nanotructures were displayed clearly. The terraces and steps further shows that the three-dimensional structures of γ-MnO_2 have a nearly hexagonal contour and are composed of thin nanoplates, which arranges regularly with the upper-bottom planes of each thin nanoplates superposing together. There are also some shedding of fragments that have anomalous shape scattered adjacently, which indicates that the thickness of the nanoflakes is about 20-30 nm. In fact, the nanoflakes with anomalous shape are may be resulted from the broken thin nanoplates due to the ultrasonication or mechanical grinding.

The lattice fringes were clearly observed from a representative high-resolution transmission electron image of the γ-MnO_2 platelet (Fig. 2c). The distances between the neighbouring lattice fringes are around 2.42 Å, which corresponds to the d-spacing of the (131) crystal planes of the γ-phase. The corresponding electron diffraction pattern (Fig. 2d) taken from the same individual nanosheet shows the single-crystalline structure. The diffraction spots can be indexed as the (131) reflections of orthorhombic γ-MnO_2. All of these data show that the as-synthesized hexagonal MnO_2 nanoplate is a single crystal and has high crystallinity. Yang *et al.*[21] and Xie's groups[22] have also reported similar hexagonal symmetric electron diffraction spots and morphology when refluxing the aqueous solution containing BrO_3^- or MnO_4^-. However, the γ-MnO_2 platelets are irregular nanosheets and have large dimension with an edge length ranging from 800 nm to 2 μm and assembled in the form of stacked hexagonal plates, no monolayer plates existent.

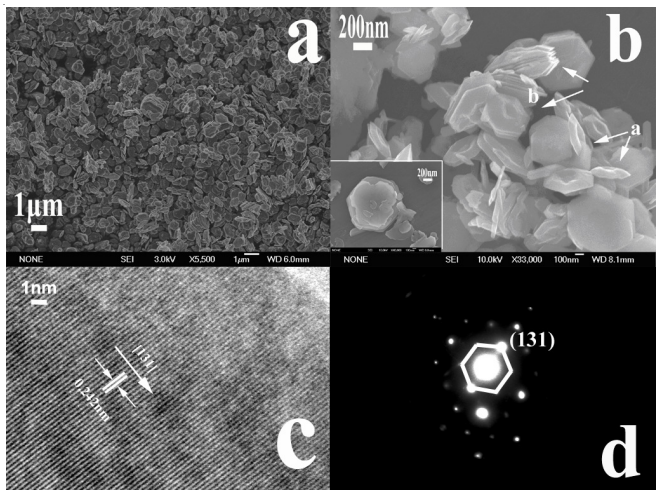

Fig. 2. (a) Low-magnification scanning electron images of γ-MnO_2 hexagonal nanoplates. (b) Enlarged scanning electron images displaying detailed structures of the hexagonal nanoplates clearly show the monolayer saucer-shaped γ-MnO_2 hexagonal nanoplates and multilayered three-dimensional structure with saucer-shaped concave on the topside layers (arrow a and b), inset of figure gives a magnified typical images of individual γ-MnO_2 multilayered three-dimensional hexagonal structure. (c) The high-resolution transmission electron image of γ-MnO_2 platelet. (d) Corresponding electron diffraction pattern of γ-MnO_2 platelet

Growth Mechanism of the as-obtained hexagonal nanoplates nanostructures: To better understand the formation mechanism, samples obtained at different stages of (a) 1 h, (b) 2 h, (c, d) 4 h, (e) 48 h and (f) 96 h were examined by scanning electron microscopy (Fig. 3a-f).

The detailed growth process was described as follows. When the reaction had proceeded for 1 h, it displayed the exclusive nanoparticles with sizes ranging from 500 nm to 2 μm. Then, after 2 h, there were some steps on the side of those nanoparticles and the edges of nanoparticles became rough. When the reaction time was 4 h, the nanoparticles shown in Fig. 3b were difficult to find, but many layered plates can be observed. Most of the nanoplates do not display the quite hexagonal in shape but contain additional fringes, which in fact consists of nanorods. All the nanorods stick out from one edge of plates and lead to the formation of the coexistence nanostructures of plates and rods (Fig. 3d). Up to about 20 h of hydrothermal treatment, most of attached nanorods disappeared, the X-ray diffraction of samples is orthorhombic phase of γ-MnO_2 structures evidence that the conversion to γ-MnO_2 nanoplates is complete. In order to further understanding about MnO_2 nanoplates evolution process under the current experi-

mental conditions, we prolonging the reaction time to 48 h and 96 h, respectively. For the reaction time of 48 h, the shape of MnO_2 nanoplates as demonstrated in Fig. 3e, became irregular or quasi-circular and had many short rod-like particles. The X-ray diffraction patterns of samples in this period have very poor quality with complex and low intensity sharp lines on top of a diffuse background, we can only surmise that they are formation of some amorphous materials instead of a pure phase of γ-MnO_2 according to the subsequent phase conversion. However, when we increase hydrothermal treatment time to 96 h, numerous micropolyhedrons are obtained and the length of their edge ranges from 1μm to 3 μm (Fig. 3f), but there are still some small particles exist. The X-ray diffraction pattern shows that they are β-MnO_2.

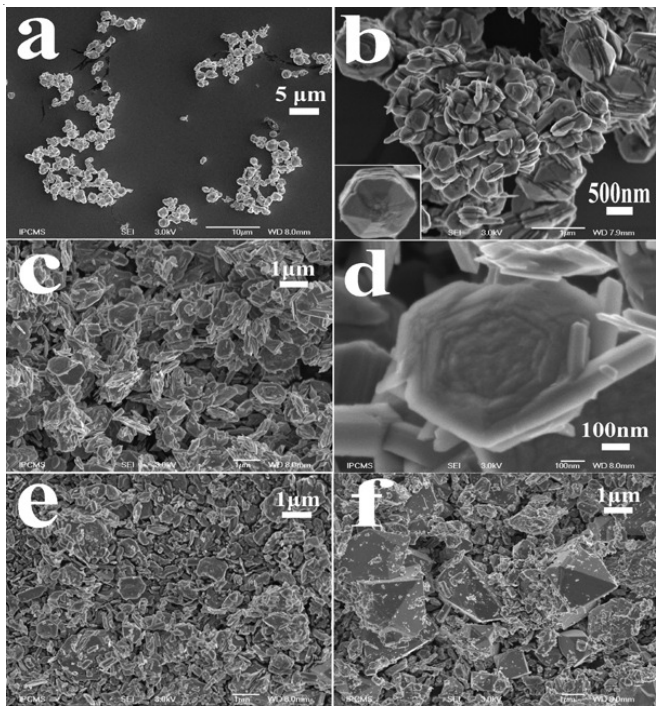

Fig. 3. A set of scanning electron micrographs of samples obtained at different growth stages of hydrothermal treating for: (a) 1 h; (b) 2 h; (c, d) 4 h; (e) 48 h; (f) 96 h

Given the above experimental results and structural information provided by electron microscopy, a possible growth mechanism is proposed to explain the formation of the saucer-shaped hexagonal γ-MnO_2 nanoplates and it was shown as follows:

(1) At the beginning of the redox reaction, the rapid increase in the temperature of the solution from room temperature to 180 ºC under the hydrothermal synthesis condition leads to a fast reaction between $Mn(NO_3)_2$ and $NaClO_3$. Normally, the produced MnO_2 colloids aggregated and formed nanospheres in solution at the early stage of reaction according to the possible oxidation reaction[23]:

$$3Mn^{2+} + ClO_3^- + 3H_2O \rightarrow 3MnO_2 + Cl^- + 6H^+$$

(2) With the continuing of reaction, the reaction rate reduced due to the decrease of the concentration of reactants in solution. When the monomer depleted, the dissolution-recrystallization process will become dominant. Therefore, the deposition of MnO_2 nanoparticles would follow the most energetically favourable direction, which exhibited that MnO_2 nanoparticles gradually changed from nanoparticles to irregular quasi-hexagonal nanoplates with some nanorods in the edge of the plate. This phenomenon suggested that these nanoparticles were dissolved and the recrystallization occurred both around the nanoparticles boundaries and the edges of plates.

(3) In surface chemistry context, it is recognized that nanoparticles have different crystal planes and each plane has a different surface energy. The growth tendency varies according to the different crystal planes. On the top of surfaces of hexagonal nanoplates, The existence of defects (such as kinks and steps) which have higher surface energies has a strong tendency to capture monomers from the mother liquor in order to reduce their surface energy, which leads to the dislocation and subsequent spiral growth along the direction perpendicular to the radial[24]. Once the first layer was formed, it may direct the growth of another layer. These particles and some early-formed plates may serve as a seed or template to promote the growth of the building blocks for those multilayered three-dimensional microparticles and steps were formed as a result.

(4) The central part of the hexagonal nanoplates may have lower surface energies by contrast with those kinks and steps. Therefore, when the monomer depleted, especially the small source nanoparticles have less mobility and diffusivity compared with atomic or ionic ingredients. The central part of the hexagonal nanoplates may not be accessible to most of the source materials. Thus, a concave on the top surface of each microparticle were formed and an increasing contour of height from the centre to the fringe occurs[25], which leaded to formation of novel saucer-shaped hexagonal nanoplates.

(5) On the basis of shape evolution observed in our results and the above discussions, it was reasonable to conclude that the reactions followed a typical nucleation-dissolution-anisotropic growth-recrystallization mechanism[23]. This dissolution-recrystallization process might last for several hours. Finally, with prolonging the reaction time, the thermodynamically controlled process should be dominated since the hydrothermal conditions can provide sufficient energy. So when the reaction time was prolonged to 48h and 96h, particles tend to minimize the surface energy through the transformation from the highly faceted hexagonal γ-MnO_2 nanoplates to β-MnO_2 micropolyhedrons structures, which possess lower specific surface area than hexagonal γ-MnO_2 nanoplates. Based on these discussions, we can deduce that those plates' morphologies and nanostructures are thermodynamically metastable structures. If the reaction time was kept enough long, the final product showed the thermodynamically favoured β-MnO_2 micropolyhedrons shapes since the long growth time can result in more thermodynamically stable shaped crystals[26].

Conclusion

In summary, we have succeeded in synthesizing well-defined hexagonal nanoplates of orthorhombic γ-MnO_2 with the side length of 250 mm and thickness of only several tens of nanometers *via* a simple aqueous chemical route without the use of any organic templates. The shape evolution suggests that the saucer-shaped hexagonal γ-MnO_2 nanoplates synthesized

follow a nucleation-dissolution-anisotropic growth-recrystallization mechanism. Due to its easily controllable reaction condition and the relatively cheap reactant sources, this synthetic approach offers great opportunities for bulk synthesis of γ-MnO_2 plates and the as-prepared nanoplates might be a promising material for battery industry.

ACKNOWLEDGEMENTS

This work is supported by the President Fund of Xi'an Technological University, China (No. XAGDXJJ1009).

REFERENCES

1. S. Iijima, *Nature*, **354**, 56 (1991).
2. R.A. Pai, R. Humayun, M.T. Schulberg, A. Sengupta, J.N. Sun and J.J. Watkins, *Science,* **303**, 507 (2004).
3. X. Wang and Y.D. Li, *J. Am. Chem. Soc*., **124**, 2880 (2002).
4. Z.Q. Li, Y. Ding, Y.J. Xiong, Q. Yang and Y. Xie, *Chem. Commun.,* **7**, 918 (2005).
5. D. Zheng, Z. Yin, W. Zhang, X. Tan and S. Sun, *Cryst. Growth Des*., **6**, 1733 (2006).
6. W.N. Li, J. Yuan, S. Gomez-Mower, S. Sithambaram and S.L. Suib, *J. Phys. Chem. B*., **110**, 3066 (2006).
7. X.F. Shen, Y.S. Ding, J. Liu, J. Cai, K. Laubernds, R.P. Zerger, A. Vasiliev, M. Aindow and S.L. Suib, *Adv. Mater*., **17**, 805 (2005).
8. F. Cheng, J. Zhao, W. Song, C. Li, H. Ma, J. Chen and P. Shen, *Inorg. Chem*., **45**, 2038 (2006).
9. N. Wang, X. Cao, L. He, W. Zhang, L. Guo, C. Chen, R. Wang and S. Yang, *J. Phys. Chem. C,* **112**, 365 (2008).
10. J. Fei, Y. Cui, X. Yan, W. Qi, Y. Yang, K. Wang, Q. He and J. Li, *Adv. Mater.,* **20**, 452 (2008).
11. X. Wang and Y. Li, *Chem. Eur. J*., **9**, 300 (2003).
12. Z.Y. Yuan, Z.L. Zhang, G.H. Du, T.Z. Ren and B.L. Su, *Chem. Phys. Lett*., **378**, 349 (2003).
13. Y. Xiong, Y. Xie, Z. Li and C. Wu, *Chem. Eur. J*., **9**, 1645 (2003).
14. J. Yuan, K. Laubernds, Q. Zhang and S.L. Suib, *J. Am. Chem. Soc*., **125**, 4966 (2003).
15. C. Wu, Y. Xie, D. Wang, J. Yang and T. Li, *J. Phys. Chem. B*., **107**, 13583 (2003).
16. S. Fritsch, E.J. Post, S.L. Suib and A. Navrotsky, *Chem. Mater*., **10**, 474 (1998).
17. S.L. Brock, M. Sanabria, S.L. Suib, V. Urban, P. Thiyagarajan and D.I. Potter, *J. Phys. Chem. B*., **103**, 7416 (1999).
18. J. Yan, Z. Fan, T. Wei, Z. Qie, S. Wang and M. Zhang, *Mater. Sci. Engg. B*, **151**, 174 (2008).
19. Z. Aia, L. Zhang, F. Konga, H. Liu, W. Xing and J. Qiu, *Mater. Chem. Phys.*, **111**, 162 (2008).
20. J.Y. Baek, H.-W. Ha, I.-Y. Kim and S.-J. Hwang, *J. Phys. Chem. C*, **113**, 17392 (2009).
21. L.X. Yang, Y.J. Zhu, W.W. Wang, H. Tong and M.L. Ruan, *J. Phys. Chem. B*, **110**, 6609 (2006).
22. C. Wu, W. Xie, M. Zhang, L. Bai, J. Yang and Y. Xie, *Chem. Eur. J*., **15**, 492 (2009).
23. D. Zheng, S. Sun, W. Fan, H. Yu, C. Fan, G. Cao, Z. Yin and X. Song, *J. Phys. Chem. B,* **109**, 16439 (2005).
24. X.Y. Liu, E.S. Boek, W.J. Brieis and P. Bennema, *Nature,* **374**, 342 (1995).
25. W.D. Shi, L.H. Huo, H.S. Wang, H.J. Zhang, J.H. Yang and P.H. Wei, *Nanotechnology*, **17**, 2918 (2006).
26. S.M. Lee, S.N. Cho and J.W. Cheon, *Adv. Mater*., **15**, 441 (2003).